Thin films of the Heusler alloys Cu_2MnAl and Co_2MnSi: recovery of ferromagnetism via solid-state crystallization from the x-ray amorphous state

2010 J. Phys. D: Appl. Phys. 43 285001

(http://iopscience.iop.org/0022-3727/43/28/285001)

IOP PUBLISHING JOURNAL OF PHYSICS D: APPLIED PHYSICS

J. Phys. D: Appl. Phys. **43** (2010) 285001 (9pp) doi:10.1088/0022-3727/43/28/285001

Thin films of the Heusler alloys Cu_2MnAl and Co_2MnSi: recovery of ferromagnetism via solid-state crystallization from the x-ray amorphous state

Denise Erb, Gregor Nowak, Kurt Westerholt and Hartmut Zabel

Institut für Festkörperphysik, Ruhr-Universität Bochum, Germany

Received 19 March 2010, in final form 27 May 2010
Published 28 June 2010
Online at stacks.iop.org/JPhysD/43/285001

Abstract

X-ray amorphous thin films of the Heusler alloys Cu_2MnAl and Co_2MnSi have been prepared by magnetron sputter deposition at room temperature. In the amorphous state the Cu_2MnAl phase is non-ferromagnetic; Co_2MnSi is weakly ferromagnetic with a ferromagnetic Curie temperature of 170 K. By solid-state crystallization at high temperatures strong ferromagnetic order and high Curie temperatures are established in both alloys. The saturation magnetization of the Co_2MnSi alloy reaches $5.1\mu_B$/f.u. at 4 K, corresponding to 100% of the theoretical value; for Cu_2MnAl we obtain $2.8\mu_B$/f.u. at 4 K, which corresponds to 87.5% of the theoretical value. In samples of the Co_2MnSi phase with optimum saturation magnetization Bragg reflections as indicators of a long-range chemical order are missing, whereas for the Cu_2MnAl phase Bragg reflections confirm epitaxial quality and long-range $L2_1$ order.

(Some figures in this article are in colour only in the electronic version)

1. Introduction

Heusler alloys are ternary intermetallic compounds of the generic composition X_2YZ. They have attracted considerable interest since their discovery about 100 years ago [1], mainly because of their versatile magnetic properties. Heusler compounds essentially exist in three crystallographically different structural variants: the ordered $L2_1$ structure with a cubic unit cell composed of four interpenetrating fcc lattices, each occupied solely by X-, Y- or Z-atoms; the B2 structure with the Y- and Z-atoms randomly occupying the Y- and Z-sublattices and the A2 structure with all four sublattices occupied at random by X-, Y- and Z-atoms, corresponding to a simple bcc lattice with random site occupancy. The magnetic properties of Heusler alloys depend sensitively on the chemical order, with the perfect $L2_1$ structure usually possessing the largest magnetic moment [2–5].

Here we report on the Heusler alloys Cu_2MnAl and Co_2MnSi: Cu_2MnAl, the original Heusler phase described by Heusler [1], may in many respects serve as a valuable model system for the complex physics of Heusler alloys, although it does not belong to the class of half metals [6]. The half-metallic phase Co_2MnSi is established as one of the most important Heusler alloys for applications. Given the highly ordered $L2_1$ structure, both Heusler alloys are strong ferromagnets with magnetic moments and ferromagnetic Curie temperatures of $3.2\mu_B$/f.u. [7] and 603 K [8] for Cu_2MnAl and $5.07\mu_B$/f.u. and 985 K for Co_2MnSi [9].

Ferromagnetic Heusler alloys experienced a striking upsurge in scientific and technological interest after the discovery of half-metallicity in some of these compounds in the early 1980s [10]: half-metallic ferromagnets—i.e. ferromagnets with full spin polarization at the Fermi level—are promising materials for applications in spintronics [11, 12]. They can be employed as spin filters [13], in spin injection/detection devices [14, 15] or in magnetic tunnelling junctions (MTJs) [16]. Apart from a few oxidic compounds and Mn-doped semiconductors [17–19], the class of Heusler alloys provides the only metallic alloy system with half-metallicity. Research on integrating half-metallic Heusler alloys into GMR thin film heterostructures is in progress [20], Co_2MnSi has been successfully employed in MTJs [21–23],

and fully epitaxial MTJs utilizing Co-based Heusler alloys have been produced recently [24, 25]. A topical review on magnetic properties of Co-based Heusler alloys can be found in [26].

The magnetic and half-metallic properties of Heusler alloys depend crucially on the atomic order [27–32], as mentioned above: true half-metallicity with a spin polarization of 100% is theoretically predicted only for perfect long-range $L2_1$ crystal structure. Therefore, the preparation of Heusler alloy thin films with $L2_1$ crystal structure is of utmost importance for optimizing the performance of Heusler alloys in spintronic devices. Perfect site order can usually best be achieved by preparing films at low growth rates and high substrate temperatures. However, high preparation temperatures are often prohibited for devices by the requirement of smooth surfaces, sharp interfaces and minimized interdiffusion. The standard preparation procedure for MTJ devices with Heusler alloy electrodes provides an illustrative example: the samples, which typically comprise seven different functional layers, are prepared by sputtering all layers in one run at room temperature, since this is the only way to obtain high-quality MgO or Al_2O_3 tunnel barriers. In the as-prepared state the Heusler alloy electrodes in these junctions exist in A2 order rather than in $L2_1$ structure. A high-temperature post-annealing procedure of the complete sample stack then establishes the magnetic moment and the high degree of spin polarization of the Heusler alloy electrodes [33]. During this annealing procedure chemical ordering or even crystallization of the Heusler alloy layers takes place. Only very few studies of these processes have been published until now [34, 35].

In section 2 we will report on how the ferromagnetism in thin films of the Heusler phases Cu_2MnAl and Co_2MnSi evolves gradually during annealing from the as-prepared, weakly magnetic state until the maximum magnetic moment is obtained. Our main objective is to describe the correlation between long-range structural order and magnetic order, and to elucidate the kinetics of the processes on the atomic level which establish this order.

2. Preparation and experimental

Thin films of the Heusler phases Cu_2MnAl and Co_2MnSi of nominally 50 nm thickness were deposited on MgO (1 0 0) and Al_2O_3 (1 1 −2 0) substrates by RF magnetron sputter deposition at room temperature from stoichiometric targets. The target diameter was 50 mm, with the distance between substrate holder and target being 80 mm. The base pressure in the UHV system was 5×10^{-9} mbar, and we used Ar at a pressure of 5×10^{-3} mbar as sputter gas. We deposited the Heusler alloy layers at very low rates of $0.003\,\mathrm{nm\,s^{-1}}$ and $0.004\,\mathrm{nm\,s^{-1}}$ for Cu and Co, by reducing the RF power to 25 W or 50 W, respectively. These low rates are essential for establishing the amorphous as-prepared state. All samples were capped by 3 nm of Al, which oxidizes in air forming a protective Al_2O_3 layer stable up to high temperatures. The stoichiometry of the films was checked by Rutherford backscattering (RBS), and found to match the nominal composition 2 : 1 : 1 within the resolution of the RBS method of about 2 at%.

MgO (1 0 0) and Al_2O_3 (1 1 −2 0) substrates induce different characteristic textures in the Heusler alloy film during its crystallization. For Al_2O_3 (1 1 −2 0) substrates one expects the (1 1 0) planes of the Heusler alloy film to be parallel to the film surface [36]; for MgO (1 0 0) the preferred orientation of the Heusler alloy film has the (1 0 0) planes parallel to the MgO (1 0 0) surface. Thus, the fundamental (2 2 0) Bragg reflection, which is already present in the chemically completely disordered A2-type Heusler alloy structure, can readily be observed in the films grown on Al_2O_3 (1 1 −2 0). For studying the (2 0 0) and (4 0 0) Bragg reflections, characterizing the B2-type of chemical long-range order, films grown on MgO (1 0 0) are best suited.

X-ray reflectometry (XRR) and diffractometry (XRD) were conducted for determining the film thickness, as well as for investigating the crystal structure of the samples, and the epitaxial relation between film and substrate. Conventional in-house fixed-anode and rotating-anode two-axes diffractometers as well as the (6+2)-circle diffractometer at the synchrotron-based beamline W1.1 at HASYLAB (DESY) were employed for these measurements. All these facilities provide radiation with a wavelength of $\lambda = 0.154$ nm, which belongs to the characteristic Cu K_α x-ray emission line. The magnetic properties of the samples were characterized by a vibrating sample magnetometer (VSM), integrated in a physical properties measurement system (PPMS, by Quantum Design). The VSM is equipped with an UHV oven (temperature range: from room temperature to 1000 K), and thus allows for an *in situ* observation of the development of the magnetic moment during thermal treatment.

Samples designated for structural characterization were annealed *ex situ* in the heating stage of the UHV sputter deposition system, whereas samples appointed for magnetic characterization underwent *in situ* thermal treatment in the VSM while measuring the sample magnetization. Since the vacuum conditions in the UHV sputter deposition system are considerably better than in the VSM, long-time annealing was only conducted in the UHV sputter deposition system.

3. Results and discussion

In figure 1 we show examples of x-ray reflectivity scans of Cu_2MnAl and Co_2MnSi thin films prepared at room temperature. The period of the well-defined total thickness oscillations corresponds to a total film thickness of 53 nm, in good agreement with the nominal thickness including the capping layer.

Interestingly, in the as-prepared sample state we could not detect any Bragg reflections in the range of high angles—irrespective of the substrate type, and even when employing the high intensity of a synchrotron radiation source (see black curves in figures 9 and 7(*a*) and (*b*)). This also holds true for the fundamental Bragg reflection (2 2 0), which already exists for Heusler alloys in the chemically completely disordered A2 structure. Thus, the chemical structure of the Heusler alloy films in the as-prepared state is amorphous or—to be

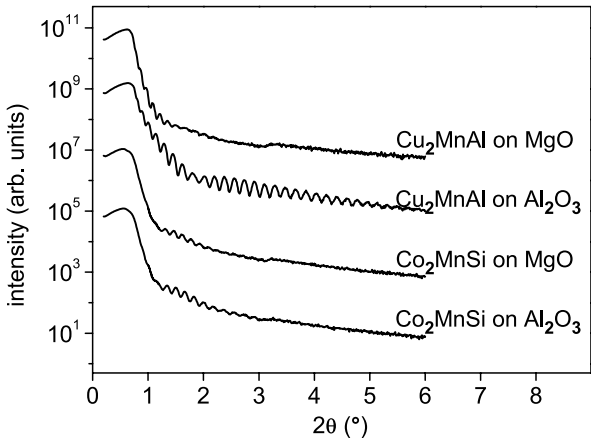

Figure 1. X-ray reflectivity scans of thin films of Cu_2MnAl and Co_2MnSi, deposited on Al_2O_3 (1 1 −2 0) and MgO (1 0 0) and capped by Al. The curves have been shifted along the *y*-axis for clarity.

more precise—x-ray amorphous; meaning that the structural coherence length is too small to yield Bragg reflections detectable by standard XRD.

3.1. Development of magnetic order

In figure 2 we depict low-temperature magnetization measurements of a Cu_2MnAl film and a Co_2MnSi film in the as-prepared state. These films were prepared on MgO (1 0 0), but virtually the same curves are obtained for films deposited on Al_2O_3 (1 1 −2 0). For Cu_2MnAl we find a weakly temperature-dependent magnetization with a magnetic moment of about $0.02\mu_B$/f.u. (see figure 2(*a*)). At 250 K the field-cooled (FC) and the zero-field-cooled (ZFC) magnetization curves begin to deviate slightly from each other, indicating the onset of magnetic irreversibility. Such a behaviour is characteristic for a spin glass order with a freezing temperature of about 250 K. Spin glass order in bulk Cu_2MnAl with A2 or B2 order has already been reported [37, 38]. Thus, in this respect an x-ray amorphous thin film of Cu_2MnAl behaves similar to disordered bulk material.

As mentioned in section 1, Cu_2MnAl in the fully ordered $L2_1$ state is a strong ferromagnet with a ferromagnetic Curie temperature of 603 K [8] and a magnetic moment of $3.2\mu_B$ at room temperature [7]. The ferromagnetism of Cu_2MnAl results from an indirect type of exchange interaction between the Mn-d orbitals, mediated by intermediate Al orbitals [6]. In the unit cell of the perfectly ordered $L2_1$ state there are no Mn nearest neighbours, whose strong antiferromagnetic exchange coupling would reduce the total magnetic moment per unit cell. In the chemically disordered A2 structure, however, nearest neighbour Mn atoms exist with a certain probability, and the strong antiferromagnetic Mn–Mn direct exchange interaction becomes relevant. The competition between the ferromagnetic and the antiferromagnetic exchange interactions in combination with random atomic disorder gives rise to magnetic frustration and spin glass type of order [39, 40].

The magnetic behaviour of the Co_2MnSi film in the as-prepared state is significantly different from that of the

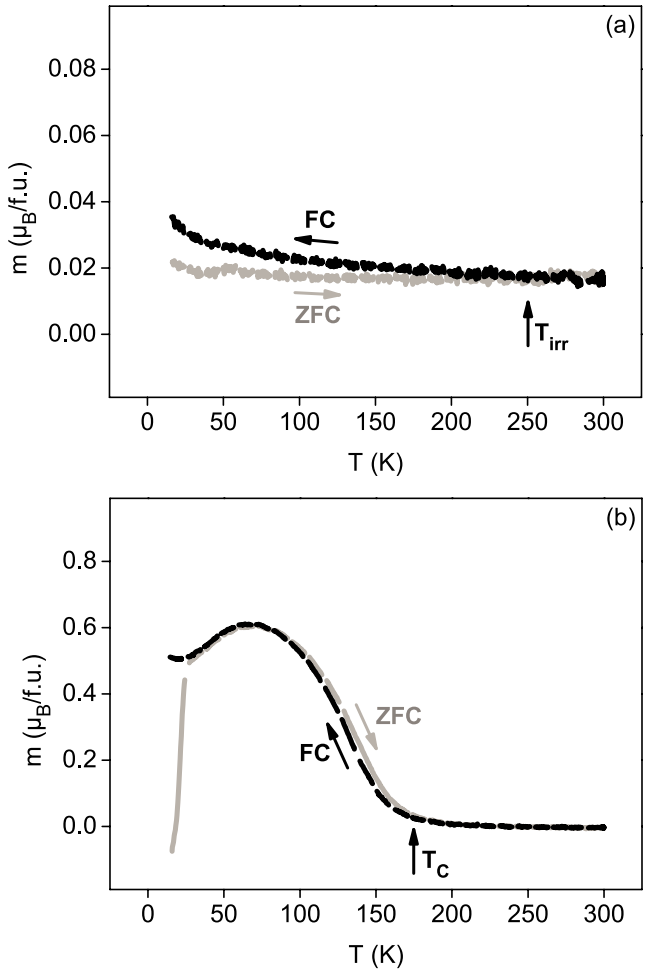

Figure 2. FC and ZFC magnetic moment versus temperature of Cu_2MnAl (*a*) and Co_2MnSi (*b*) thin films grown on MgO (1 0 0) in the as-prepared state, measured in an external field of $H = 200$ Oe. The arrows indicate the direction of the temperature variation.

Cu_2MnAl film (see figure 2(*b*)): we observe a ferromagnetic type of $M(T)$-curve with a ferromagnetic Curie temperature of about 170 K, and typical ferromagnetic hysteresis loops below this temperature. The saturation magnetic moment reaches $0.6\mu_B$/f.u. at low temperatures. In addition, below a temperature of about 31 K, a strong magnetic irreversibility sets in—as evidenced by the sudden deviation of the FC and ZFC magnetization curves at 31 K. This behaviour is typical for re-entrant ferromagnetism [41].

In comparison, Co_2MnSi in the fully ordered $L2_1$ state has a ferromagnetic Curie temperature of 985 K—which is actually one of the highest Curie temperatures ever detected within the family of Heusler alloys [5]—and a magnetic moment of $5.07\mu_B$/f.u. [9]. Thus, Curie temperature and magnetic moment of the as-prepared Co_2MnSi film are drastically reduced as compared with the values in the chemically ordered $L2_1$ state. This observation can qualitatively be explained following the same lines of argument as for the Cu_2MnAl phase: in the x-ray amorphous state with a short-range A2-type of atomic order strong antiferromagnetic interactions between nearest neighbour Mn atoms compete with ferromagnetic Co–Mn and Co–Co interactions [42], thus the average total

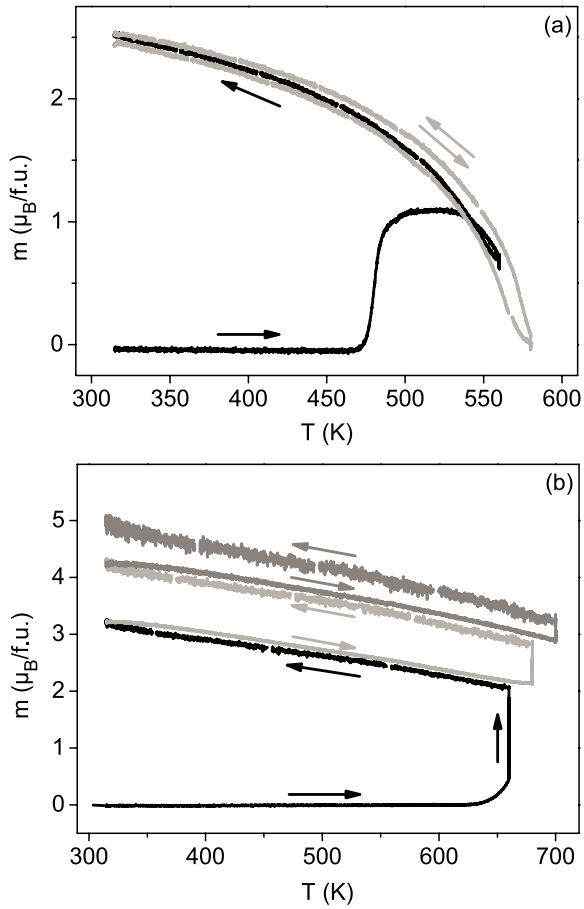

Figure 3. Magnetic moment versus temperature for (*a*) Cu_2MnAl and (*b*) Co_2MnSi thin films grown on Al_2O_3 (1 1 −2 0), recorded *in situ* during thermal cycling (see the main text) in an external field of $H = 1$ kOe. The direction of the arrows indicates the direction of the temperature variation; the temperature was kept constant for 1 h at the maximum temperature during each cycle.

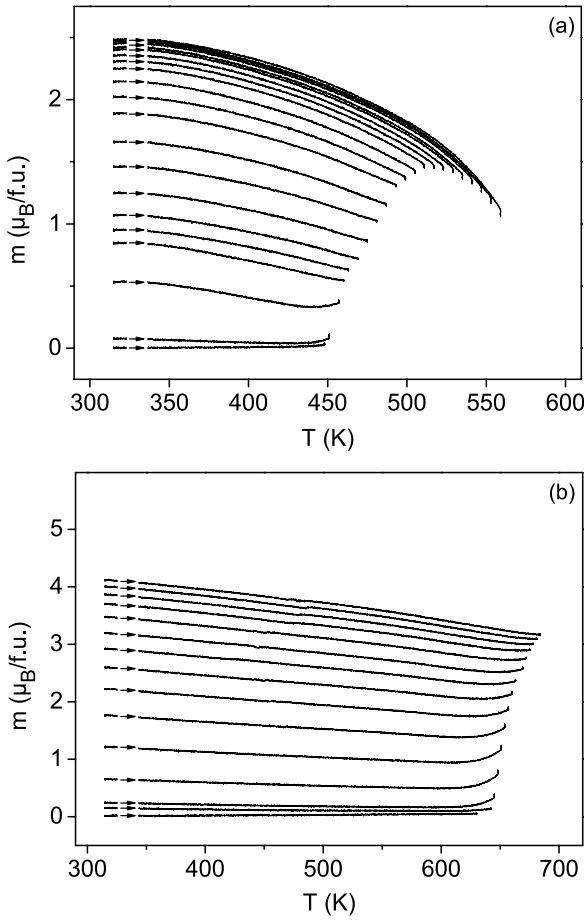

Figure 4. Magnetic moment versus temperature for (*a*) Cu_2MnAl and (*b*) Co_2MnSi thin films grown on Al_2O_3 (1 1 −2 0) during sequential annealing (see the main text) in an external field of $H = 1$ kOe. During each step of the sequence the samples were heated up to the respective maximum temperature at a rate of 5 K min^{-1} and rapidly quenched to room temperature. Only the magnetic moment measured during the heating branch is shown.

magnetic moment per formula unit is diminished. In contrast to the situation in Cu_2MnAl, there are two magnetic atoms in the unit cell of Co_2MnSi: Mn contributing about $3\mu_B$ and Co contributing about $1\mu_B$ per atom [43]. Since the majority of the magnetic interactions in the unit cell are ferromagnetic, a finite ferromagnetic magnetization remains even in the case of complete chemical disorder. However, the magnetic ground state is not purely ferromagnetic, but random spin disorder coexists with ferromagnetic order: such a situation is characteristic for the re-entrant ferromagnetism observed in the vicinity of the ferromagnetic and spin glass phase boundaries of systems with competing magnetic interactions [41].

In figure 3 we show high-temperature magnetization measurements recorded *in situ* during thermal treatment of Cu_2MnAl and Co_2MnSi thin films. The thermal treatment comprises two cycles for Cu_2MnAl (see figure 3(*a*): the black curve corresponds to first cycle, the grey curve corresponds to the second cycle) and three cycles for Co_2MnSi (see figure 3(*b*): the black curve corresponds to the first cycle, the light grey curve to the second cycle and the dark grey curve corresponds to the third cycle). In each cycle the sample was heated up from room temperature to a specific annealing temperature at a constant rate of 5 K min^{-1}. After annealing the films for 1 h per cycle, the samples were cooled back down to room temperature at a rate of −5 K min^{-1}. The films for the measurements shown in figure 3 have been grown on Al_2O_3 (1 1 −2 0), but films grown on MgO (1 0 0) show virtually identical behaviour.

For Cu_2MnAl the initial magnetization at room temperature is very small, because the sample is non-ferromagnetic in the as-prepared state (see figure 3(*a*)). The magnetization increases rapidly for temperatures above 480 K, and quickly reaches typical ferromagnetic magnetization values of about $1\mu_B$/f.u. The formation of the ferromagnetic state out of the x-ray amorphous as-prepared state is accomplished by an irreversible solid-state crystallization and chemical ordering process. Upon cooling we observe a typical ferromagnetic magnetization curve, which extrapolates to a Curie temperature of about 600 K and to a ferromagnetic saturation moment of $2.5\mu_B$/f.u. at room temperature.

For Co_2MnSi the magnetization curve recorded during the heating of the film from the as-prepared state up to 660 K (black curve in figure 3(*b*)) principally exhibits a behaviour very similar to that observed for Cu_2MnAl. However, the irreversible transition to the ferromagnetic state is shifted to

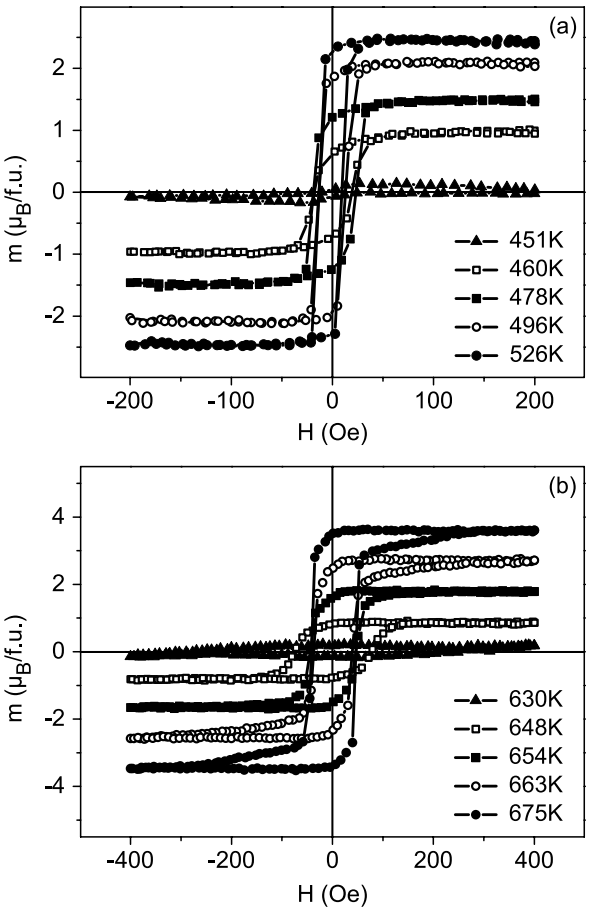

Figure 5. Magnetic hysteresis loops of (*a*) Cu_2MnAl and (*b*) Co_2MnSi thin films grown on Al_2O_3 (1 1 −2 0), measured at room temperature after quenching from the temperatures given in the figure during the sequential annealing procedure described in the main text (see also figure 4).

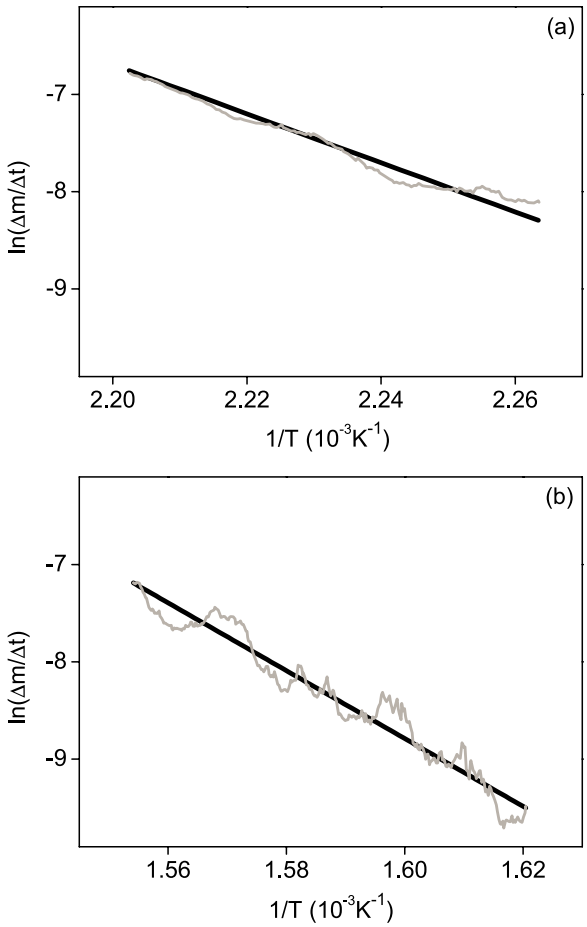

Figure 6. Logarithm of the absolute value of the temporal derivative of the magnetization versus the reciprocal temperature for (*a*) Cu_2MnAl and (*b*) Co_2MnSi grown on MgO (1 0 0). The slope of the straight line defines the thermal activation energy.

higher temperatures. The onset of ferromagnetic order is observed at 640 K only—as compared with 480 K for the Cu_2MnAl phase. Thus, the thermal activation energy involved in the crystallization process is definitely higher in Co_2MnSi than in Cu_2MnAl. After annealing the sample at 660 K for 1 h, we observe a typical ferromagnetic $M(T)$-curve upon cooling to room temperature. The recorded magnetization curve is compatible with a ferromagnetic Curie temperature well above 900 K and with a saturation magnetic moment of $3.2\mu_B$/f.u. at room temperature.

For the observation of the irreversible structural changes via the *in situ* measurement of the magnetization shown in figure 3 we have applied a magnetic field of $H = 1$ kOe. Analogous measurements in fields of $H = 200$ Oe and $H = 50$ kOe, respectively, yielded virtually the same temperatures for the onset of the irreversible structural changes. Thus, the applied magnetic field has no direct influence on this development.

In figure 4 we depict a series of magnetization measurements, in which the samples are subsequently heated to higher and higher temperatures and quenched to room temperature while applying a constant external field of $H = 1$ kOe. Thereby we demonstrate that the saturation magnetization of both Heusler phases can be tuned to any value between zero and full saturation magnetic moment.

Figure 5 shows the corresponding magnetic hysteresis loops measured at room temperature after quenching from a specific high temperature. The hysteresis loops have a nearly rectangular shape with small coercive fields of about $H_c \approx 10$ Oe for Cu_2MnAl and $H_c \approx 50$ Oe for Co_2MnSi, essentially independent of the degree of magnetic order established in the sample. These coercive forces seem exceptionally small as compared with those in thin films of the same Heusler phases prepared at high temperatures [44], and indicate an excellent magnetic homogeneity of the films.

We have also tested systematically the maximum magnetic moment which we can achieve by long-time annealing treatment of the samples at high temperatures: for the Cu_2MnAl phase we could not improve the maximum magnetization, which was already obtained after annealing at 560 K and at 580 K for 1 h each. The maximum saturation magnetic moment was $2.5\mu_B$/f.u. at room temperature and $2.8\mu_B$/f.u. at 4 K, which corresponds to 87.5% of the value for bulk Cu_2MnAl [7]. Prolonging the annealing time or increasing the annealing temperature above 600 K is counterproductive, i.e. it lowers the maximum saturation magnetic moment.

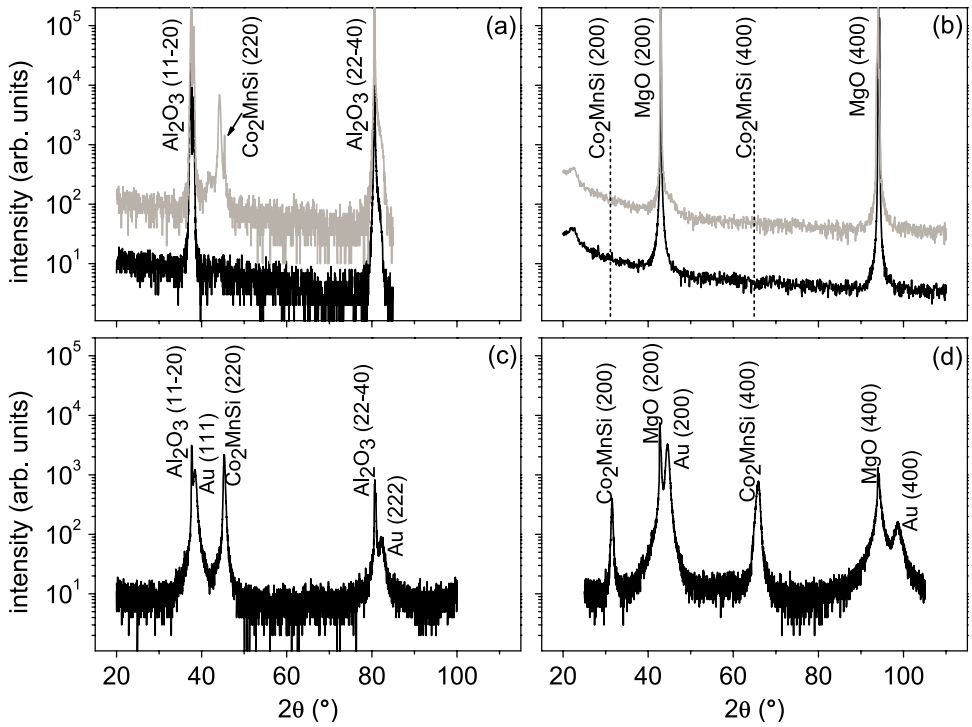

Figure 7. Out-of-plane x-ray diffraction patterns for Co_2MnSi thin films: (*a*), (*b*) deposited at room temperature (black curve) and annealed for 10 h at 730 K (grey curve), recorded at HASYLAB and at a rotating-anode in-house facility, respectively; (*c*), (*d*) deposited at 770 K with an Au capping layer of 5 nm thickness, recorded at a fixed anode in-house facility. Panels on the left-hand side show films deposited on Al_2O_3 (1 1 −2 0); panels on the right-hand side show films deposited on MgO (1 0 0).

For the Co_2MnSi phase we could increase the maximum saturation magnetic moment significantly by annealing the films at 700 K for 1 h; the corresponding magnetization curve has been included in figure 3(*b*) (dark grey curve). The saturation magnetic moment, which we achieved for Co_2MnSi after this heat treatment, was $4.9\mu_B$ at room temperature and $5.1\mu_B$/f.u. at 4 K, which corresponds to the maximum magnetic moment expected theoretically for this phase in the perfectly ordered $L2_1$ structure [9].

3.2. Thermal activation energies

The irreversible change in the magnetization of the Cu_2MnAl and Co_2MnSi thin films at high temperatures is caused by atomic nearest neighbour hopping processes in the Heusler compound unit cell. Therefore, it appears sensible to assume that a proportionality exists between the initial change in the ferromagnetic magnetization $\triangle M(T)$ and the probability for nearest neighbour hopping $p(T)$. With the reasonable assumption of an Arrhenius law for the temperature dependence of the probability for nearest neighbour hopping processes $p(T) = p_0 \exp(-E_a/k_B T)$ we can thus assume that

$$\triangle M(T,t) \propto t \cdot \exp(-E_a/k_B T)$$

with the heating time t and the thermal activation energy E_a. In figure 6 we show corresponding Arrhenius plots for Cu_2MnAl and Co_2MnSi, deduced by numerical differentiation of magnetization data shown in figure 4. From the straight line fits in figure 6 we derive thermal activation energies E_a of 2.2 eV and 3.0 eV for Cu_2MnAl and Co_2MnSi, respectively, which are reasonable values for nearest neighbour hopping processes in metals.

3.3. Development of chemical order in Co_2MnSi

As stated at the beginning of this section, there are no detectable Bragg peaks in the XRD patterns of samples in the as-prepared state. This observation has led us to the conclusion that before thermal treatment the samples are in an x-ray amorphous state, i.e. the coherence length of their structural order is too small to yield detectable Bragg reflections. After annealing Co_2MnSi films for an accumulated time of 3 h at temperatures ranging from 660 to 700 K (see figure 3(*b*)), the XRD patterns still show no Bragg reflections, although the sample is already ferromagnetic with a ferromagnetic saturation moment close to the theoretical limit. As discussed above, a reduction in the number of antiferromagnetically coupled Mn nearest neighbours is sufficient for the occurrence of ferromagnetism with large saturation moments in Heusler compounds. This can be achieved by some re-arrangement of the site occupancy within the unit cell via nearest neighbour hopping processes.

Eventually, after further annealing the sample for 10 h at 730 K, a (2 2 0) Bragg reflection indicating long-range A2 order could be detected for the Co_2MnSi film grown on Al_2O_3 (1 1 −2 0) (see figure 7(*a*)). However, there are two additional peaks at $2\Theta = 44.2^\circ$ and at $2\Theta = 42.3^\circ$, respectively, which do not belong to the Heusler phase, but suggest a decomposition of the film. This is corroborated by the change in the ferromagnetic hysteresis loops after this high-temperature annealing, as depicted in figure 8(*a*): the

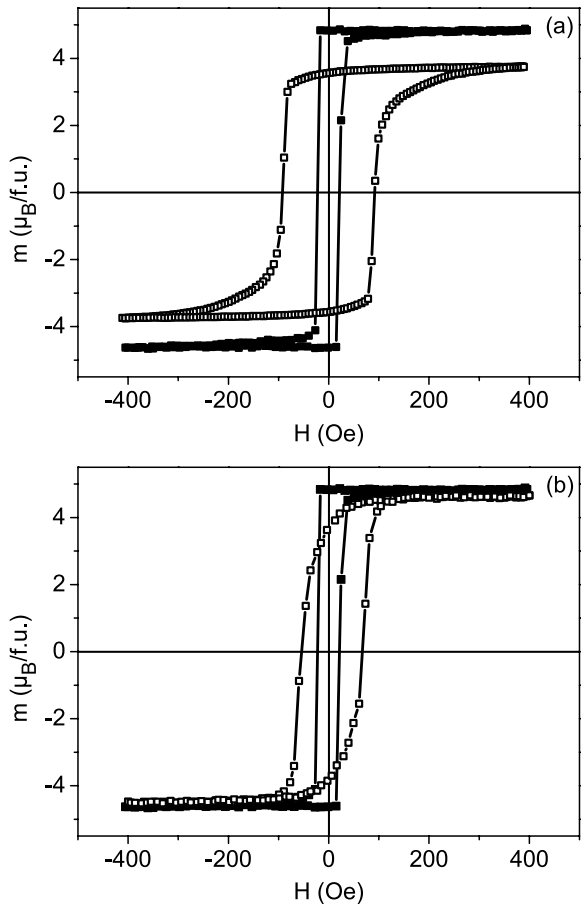

Figure 8. Hysteresis curves of Co_2MnSi thin films (*a*) annealed from the amorphous as-prepared state for 3 h at 660 to 700 K (full symbols) and additionally annealed for 10 h at 730 K (open symbols), (*b*) annealed from the amorphous as-prepared state for 3 h at 660 K to 700 K (full symbols) and deposited at 770 K without subsequent annealing (open symbols).

saturation magnetization is definitely lowered, and the coercive field is clearly increased as compared with the sample state which is obtained after annealing at lower temperatures (see figure 3(*b*)). We did not try to identify the impurity phases formed during the decomposition at 730 K. The precipitation of fcc Co from the Co_2MnSi Heusler phase at high temperatures has been suggested in the literature [45].

Given a long-range $L2_1$ structural order, the (2 0 0) and (4 0 0) reflections are expected to be displayed in out-of-plane Bragg scans of Co_2MnSi films deposited on MgO (1 0 0). These reflections remain absent, even after annealing at 730 K for 10 h (see figure 7(*b*)). Thus, only A2-type of long-range structural order has been formed; the coherence length of B2- and $L2_1$-type of long-range order still does not exceed the sensitivity limit of standard x-ray Bragg diffraction. In figures 7(*c*) and (*d*) we depict Bragg scans for Co_2MnSi films grown on Al_2O_3 (1 1 −2 0) and on MgO (100) at a substrate temperature of 770 K for comparison. For these films we observe the (2 2 0) Bragg reflection on Al_2O_3 (1 1 −2 0) as well as the (2 0 0) and (4 0 0) Bragg reflections on MgO (1 0 0). However, concerning the magnetic properties of these films, there is not much of a difference due to the alternative preparation conditions; the films prepared via the amorphous state even exhibit a slightly larger saturation magnetization and smaller coercive field (see figure 8(*b*)).

3.4. Development of long-range chemical order in Cu_2MnAl

The results of our XRD studies on Cu_2MnAl differ significantly from those discussed above for the Co_2MnSi films in several respects: after annealing Cu_2MnAl films for 1 h at a moderate temperature of 580 K, the out-of-plane XRD patterns already show the characteristic Bragg reflections for this phase (see figures 9(*a*) and (*b*)). For the film prepared on MgO (1 0 0) we observe well resolved (2 0 0) and (4 0 0) Bragg reflections, indicating the expected texture for [1 0 0] growth on MgO (1 0 0). The (2 0 0) superstructure reflection originates from a substantial degree of long-range B2-type of chemical order (i.e. separation of Mn atoms and Al atoms on their respective sublattices). From the full width at half maximum (FWHM) of these Bragg peaks we can derive the structural coherence length ξ by applying the Scherrer formula; we obtain a value of about $\xi = 25$ nm, corresponding to 50% of the total film thickness. The rocking width of the (4 0 0) peak correlates with a mosaic spread of 0.45° for the crystallites within the plane. Both parameters indicate a high-quality textured growth on MgO (1 0 0).

For Cu_2MnAl deposited on Al_2O_3 (1 1 −2 0) and annealed for 1 h at 580 K we observe a (2 2 0) Bragg reflection at an angle of $2\Theta = 44°$ in the out-of-plane Bragg scan, consistent with the expected [1 1 0] texture for the Heusler alloy growth on Al_2O_3 (1 1 −2 0). The intensity of the (2 2 0) peak is lower than that observed for the (2 0 0) and (4 0 0) peaks in figure 9(*a*), although the (2 2 0) peak is the fundamental Bragg reflection for the Heusler compounds, and therefore is expected to have the highest intensity. Moreover, the mosaic spread of more than 2 for Cu_2MnAl grown on Al_2O_3 (1 1 −2 0) is significantly larger than for Cu_2MnAl on MgO (1 0 0); thus the structural quality of the Cu_2MnAl phase when grown on Al_2O_3 (1 1 −2 0) is clearly lower than when grown on MgO (1 0 0). Although after crystallization and thermally induced chemical order the resulting structural qualities of the Heusler phases deposited on MgO (1 0 0) and on Al_2O_3 (1 1 −2 0) differ markedly, the ferromagnetic properties are very similar.

The Cu_2MnAl films deposited on MgO (1 0 0) even have epitaxial film quality after annealing at 580 K for 1 h, as proven by the in-plane azimuthal scans in figure 10, which were recorded employing synchrotron radiation. The in-plane 360° azimuthal scans on the Heusler (4 0 0) Bragg reflection and the MgO (2 0 0) Bragg reflection demonstrate the perfect four-fold symmetry of the crystal structure of this film, with the Heusler (4 0 0) Bragg peaks shifted by 45° from the MgO (2 0 0) Bragg peaks. This corresponds to an in-plane epitaxial relation between substrate and film with the [1 0 0] direction of the Heusler phase rotated by 45° from the [1 0 0] direction of the MgO substrate. For this film we also conducted an in-plane 360° azimuthal scan on the asymmetric (1 1 1) Bragg reflection, which is tilted in the scattering plane by 26.14 with respect to the sample surface. This reflection unambiguously identifies the $L2_1$-type of chemical order in Heusler alloys. The results presented in figure 10(*b*) again reflect the perfect

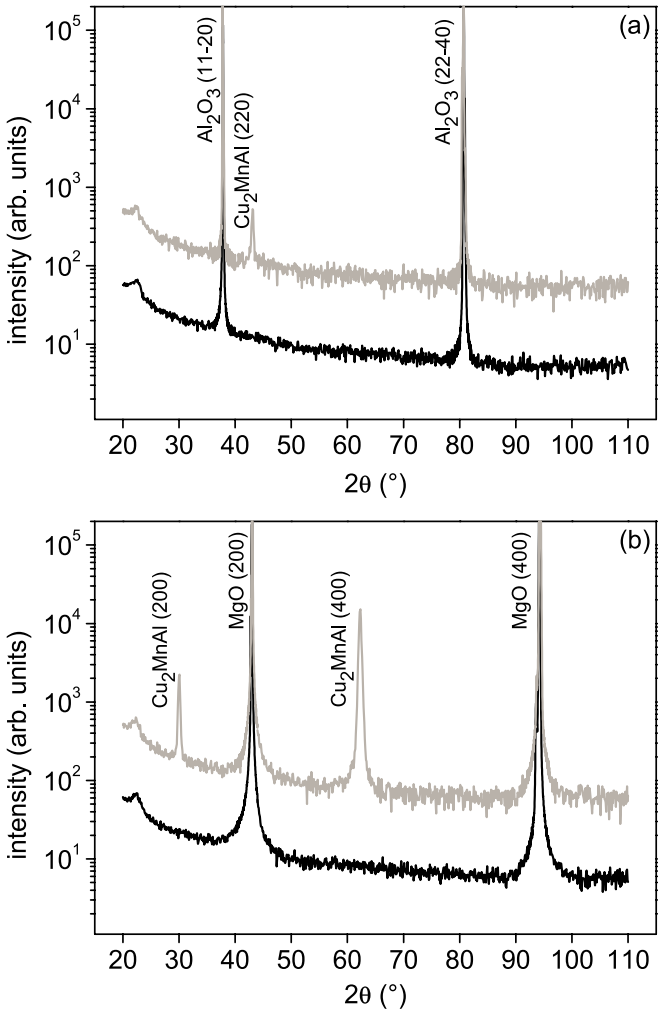

Figure 9. Out-of-plane x-ray diffraction patterns of Cu_2MnAl thin films deposited on (*a*) Al_2O_3 (1 1 −2 0) and (*b*) MgO (1 0 0), in the as-prepared state (black curves) and after annealing for 1 h at 560 K (grey curves). Recorded at a rotating-anode in-house facility.

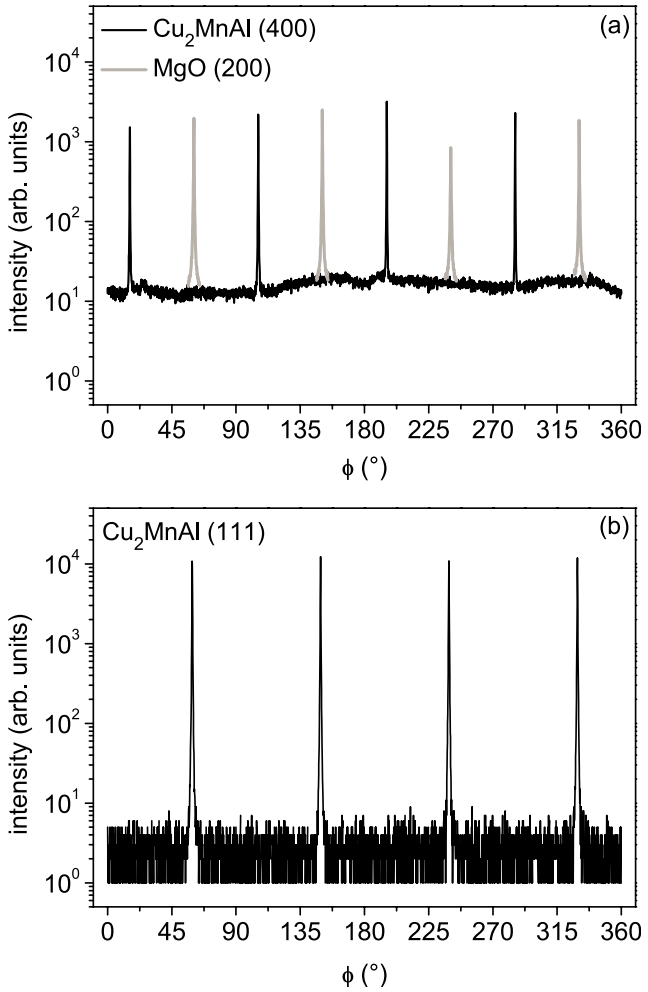

Figure 10. In-plane 360 azimuthal scans on the (4 0 0) Bragg reflection (*a*) and on the asymmetric (1 1 1) reflection (*b*) of the Cu_2MnAl thin film from figure 9(*b*). Recorded at HASYLAB.

cubic symmetry of the film. Moreover, they prove that the film possesses an appreciable degree of long-range $L2_1$ order.

4. Summary and conclusions

We have shown in this investigation that thin films of the Heusler alloys Cu_2MnAl and Co_2MnSi grown by magnetron sputtering at room temperature and at very low deposition rates are x-ray amorphous and non-ferromagnetic. Annealing of the as-prepared state establishes strong ferromagnetism via solid-state crystallization and atomic ordering. Atomic nearest neighbour hopping processes within the unit cell of the disordered Heusler phases create a short-range chemical order, which is the prerequisite for the ferromagnetic state. For both Heusler alloys we obtained large ferromagnetic saturation magnetic moments; the hysteresis curves are of a square type with very low coercive field values.

The degree of atomic long-range order was probed by XRD before and after heat treatment, revealing for the Co_2MnSi phase that even the sample state with the highest saturation magnetic moment yields no detectable Bragg reflections. This Heusler phase provides further evidence that chemical long-range order is not required for strong ferromagnetism—chemical short-range order is sufficient. The prototypes for this situation are amorphous ferromagnetic metals such as NiP [46] or $Fe_{80}B_{20}$ [47]. Our experimental data allow no inferences on the details of the atomic short-range order and electronic structure of the samples. Future research will provide the necessary information and will suggest explanations for the large saturation magnetic moments which can be observed in amorphous Heusler alloys.

In contrast, for Cu_2MnAl films grown on MgO (1 0 0) we achieved epitaxial film quality from the x-ray amorphous as-prepared state by short-time annealing at a moderate temperature of 580 K. The epitaxial quality of these films is comparable to that which we have obtained before by growing Cu_2MnAl films on MgO (1 0 0) at high substrate temperatures [48]. It is common belief that high substrate temperatures are necessary for single crystalline thin film growth, since high surface mobility of the atoms during the growth process is essential. Thus, it seems remarkable that for the Cu_2MnAl phase an alternative route via solid-state crystallization from an x-ray amorphous phase also leads to single crystallinity and epitaxy.

The crystallization and atomic ordering processes for Cu_2MnAl and Co_2MnSi films are significantly different. For the Co_2MnSi phase it is easy to establish a high magnetic moment, but very difficult to achieve any type of crystalline long-range order. Actually, an annealing temperature of 730 K was required before we could observe at least the fundamental (2 2 0) Bragg reflection. However, the Co_2MnSi films decompose under these conditions. In contrast, long-range structural order is readily established in Cu_2MnAl thin films. The main reason for this striking difference is the fact that the activation energy in Co_2MnSi is much larger than in Cu_2MnAl. We assume that due to the covalent character of the Si metal bonds the Si atoms in the Co_2MnSi unit cell are nearly immobile at the temperatures applicable, so that the system can hardly remove the frozen-in atomic disorder on a long-range scale. As a compromise, only chemical short-range order is formed during annealing. However, this is sufficient to establish a magnetic saturation moment reaching that predicted by theory for perfectly ordered $L2_1$ symmetry.

Acknowledgments

The authors wish to acknowledge financial support of this work within SFB 491 by the DFG. They thank P Stauche and S Erdt-Bhm for technical assistance with the sputter deposition as well as Dr H J Becker and Dr D Rogalla for conducting the RBS measurements. They would also like to acknowledge support by W Caliebe at the HASYLAB beamline W1.1.

References

[1] Heusler F 1903 *Verh. Dtsch. Phys. Ges.* **5** 219
[2] Persson E 1929 *Z. Phys.* **57** 115
[3] Potter H H 1929 *Proc. Phys. Soc. London* **41** 135
[4] Bradley A J and Rodgers J W 1934 *Proc. R. Soc.* A **144** 340
[5] Webster P J and Ziebeck K R A 1988 *Alloys and Compounds of d-Elements with Main Group Elements* part 2 ed H R J Wijn (Landolt-Börnstein, New Series, Group III) vol 19c (Berlin: Springer) pp 75–184
[6] Kübler J, Williams A R and Sommers C 1983 *Phys. Rev.* B **28** 1745
[7] Felcher G P, Cable J W and Wilkinson M 1963 *Phys. Chem. Solids* **24** 1663
[8] Oxley D, Tebble R and Williams K 1963 *J. Appl. Phys.* **34** 1362
[9] Webster P J 1971 *Phys. Chem. Solids* **32** 1221
[10] de Groot R A, Mueller F M, van Engen P G and Buschow K H J 1983 *Phys. Rev. Lett.* **50** 2024
[11] Felser C, Fecher G H and Balke B 2007 *Angew. Chem. Int. Edn* **46** 668
[12] Zabel H 2009 *Superlatt. Microstruct.* **46** 541
[13] Kilian K A and Victora R H 2000 *J. Appl. Phys.* **87** 7064
[14] Datta S and Das B 1990 *Appl. Phys. Lett.* **56** 665
[15] Hickey M C, Damsgaard C D, Holmes S N, Farrer I, Jones G A C, Ritchie D A, Jacobsen C S, Hansen J B and Pepper M 2008 *Appl. Phys. Lett.* **92** 232101
[16] Tanaka C T, Nowak J and Moodera J S 1999 *J. Appl. Phys.* **86** 6239
[17] Ji Y, Strijkers G J, Yang F Y, Chien C L, Byers J M, Anguelouch A, Xiao G and Gupta A 2001 *Phys. Rev. Lett.* **86** 5585
[18] Park J-H, Vescovo E, Kim H-J, Kwon C, Ramesh R and Venkatesan T 1998 *Nature* **392** 794
[19] Stroppa A, Picozzi S, Continenza A and Freeman A J 2003 *Phys. Rev.* B **68** 155203
[20] Caballero J A, Park Y D, Childress J R, Bass J, Chiang W-C, Reilly A C, Pratt W P Jr and Petroff F 1998 *J. Vac. Sci. Technol.* A **16** 1801
[21] Hütten A, Kämmerer S, Schmalhorst J, Thomas A and Reiss G 2004 *Phys. Status Solidi* a **201** 3271
[22] Reiss G, Hütten A, Kämmerer S and Schmalhorst J 2006 *Phys. Status Solidi* c **3** 1322
[23] Sakuraba Y, Hattori M, Oogane M, Ando Y, Kat H, Sakuma A, Miyazaki T and Kubota H 2006 *Appl. Phys. Lett.* **88** 192508
[24] Yamamoto M, Marukame T, Ishikawa T, Matsuda K, Uemura T and Arita M 2006 *J. Phys. D: Appl. Phys.* **39** 824
[25] Kijima H, Ishikawa T, Marukame T, Matsuda K-I, Uemura T and Yamamoto M 2007 *J. Magn. Magn. Mater.* **310** 2006
[26] Trudel S, Gaier O, Hamrle J and Hillebrands B 2010 *J. Phys. D: Appl. Phys.* **43** 193001
[27] Raphael M, Ravel B, Huang Q, Willard M A, Cheng S F, Das B N, Stroud R M, Bussmann K M, Claassen J H and Harris V G 2002 *Phys. Rev.* B **66** 104429
[28] Miura Y, Nagao K and Shirai M 2004 *Phys. Rev.* B **69** 144413
[29] Miura Y, Shirai M and Nagao K 2004 *J. Appl. Phys.* **95** 7225
[30] Picozzi S, Continenza A and Freeman A J 2004 *Phys. Rev.* B **69** 094423
[31] Gaier O, Hamrle J, Hermsdoerfer S J, Schultheiß H, Hillebrands B, Sakuraba Y, Oogane M and Ando Y 2008 *J. Appl. Phys.* **103** 103910
[32] Mizukami S, Watanabe D, Oogane M, Ando Y, Miura Y, Shirai M and Miyazaki T 2009 *J. Appl. Phys.* **105** 07D306
[33] Kämmerer S, Thomas A, Hütten A and Reiss G 2004 *Appl. Phys. Lett.* **85** 79
[34] Kim K, Kwon S-J and Kim T-W 2004 *Phys. Status Solidi* b **241** 1557
[35] Kudryavtsev Y V, Oksenenko V A, Lee Y P, Hyun Y H, Kim J B, Park J S, Park S Y and Dubovik J 2007 *Phys. Rev.* B **76** 024430
[36] Geiersbach U, Bergmann A and Westerholt K 2003 *Thin Solid Films* **425** 225
[37] Taylor R and Tsuei C 1982 *Solid State Commun.* **41** 503
[38] Krusin-Elbaum L, Malozemoff A P and Taylor R C 1983 *Phys. Rev.* B **27** 562
[39] Binder K and Young A P 1986 *Rev. Mod. Phys.* **58** 801
[40] Greedan J E 2001 *J. Mater. Chem.* **11** 37
[41] Gunnarsson K, Svedlindh P, Andersson J-O, Nordblad P, Lundgren L, Katori H A and Ito A 1992 *Phys. Rev.* B **46** 8227
[42] Galanakis I and Dederichs P H 2005 *Half-Metallic Alloys—Fundamentals and Applications Lecture Notes Phys.* vol 676 ed I Galanakis and P H Dederichs (Berlin: Springer) pp 311–49
[43] Galanakis I, Dederichs P H and Papanikolaou N 2002 *Phys. Rev.* B **66** 174429
[44] Geiersbach U, Bergmann A and Westerholt K 2002 *J. Magn. Magn. Mater.* **240** 546
[45] Kim S J, Lim D H, Yoon C S and Kim C K 2004 *Solid State Commun.* **132** 361
[46] Berrada A, Lapierre M F, Loegel B, Panissod P and Robert C 1978 *J. Phys. F: Met. Phys.* **8** 845
[47] Hasegawa R, O'Handley R C, Tanner L E, Ray R and Kavesh S 1976 *Appl. Phys. Lett.* **29** 219
[48] Bach H, Westerholt K and Geiersbach U 2002 *J. Cryst. Growth* **237–239** 2046